https://doi.org/10.32388/JC0DMR

The Application of Adjustable Magnetic Devices in Electric Power Systems

Michał Gwóźdź

Faculty of Control, Robotics and Electrical Engineering, Poznan University of Technology, Piotrowo 3A Street, 60-965 Poznan, Poland; michal.gwozdz@put.poznan.pl

Abstract: This work represents a continuation of the research cycle on magnetic devices with adjustable parameter values. The work focuses on the possibility of using tunable magnetic devices in electrical power systems with adaptive features. The idea underlying this type of operation, which depends on interaction with magnetic fluxes, is a new approach to the design of magnetic elements. Suitable examples of adaptive electric power systems can act as devices for improving the quality of electricity. When used in compensators of reactive power or both reactive and distortion power, magnetic devices in the form of tuned inductors offer much wider possibilities for the compensation of both reactive and distortion power in electric systems, compared to 'standard' solutions, involving compensators based on inductors with fixed parameter values. Nevertheless, the application of the proposed device in electric systems such as these is only one example of its possible implementations in the area of electric power. In the work, the following issues are covered: an exemplary solution of an adaptive 'passive' compensator, rules for the operation of an adjustable magnetic device, and an investigation of the results from a laboratory model of an electric system based on this device.

Keywords: adaptive compensator; converter control; quality of electricity; tunable magnetic device

List of acronyms

APC – Adaptive Passive Compensator
APF – Active Power Filter
PA – Power Amplifier
TCM – Tuned Capacitor Mode
TI – Tuned Inductor
TIM – Tuned Inductor Mode
VCVS – Voltage Controlled Voltage Source

1. Introduction

This paper focuses on the operation and possible implementation of an adjustable magnetic device in a power electronics system with adaptive features. In the following, this device is referred to as a 'tuned inductor' (TI).
The first group of these devices consists of systems for improving the quality of electricity [1–4]. A further possible area of implementation of TI solutions is in static power electronics systems, installed in AC transmission grids, as such system can increase their power transfer capability, stability, and controllability through series and/or shunt compensation. These are known as flexible AC transmission systems (FACTS) [1,5,6]. The third area concerns AC/DC, DC/AC, and DC/DC converters, which allow for shaping of the frequency characteristics of these devices [7–10]. This work focuses mainly on the application of TIs in the first group of power electric systems.
The negative effect of nonlinear loads on the operation of a power line, resulting in a lowering of the desired parameter values for the electrical energy [11], is a widely known and well-documented phenomenon. In view of this, various types of compensators, mainly consisting of different kinds of power filters, are used in these electrical systems as preventive measures [1,12–14]. The main task of these devices is to match the shape of the current at its input to the shape of the current drawn from the same grid node by other loads. As a result of this compensation process the current, flowing from the power line to the load, should have both a suitable shape and a correct phase relationship with the voltage in the power line node. This process depends on the chosen compensation strategy, relative to the reactive power alone or to the both the reactive and the distortion power [2,15–17].
The operation of a TI represents a new approach to the design of power devices with adaptive compensation. However, in this work the operation of an adaptive compensator, as a whole, is not related to any specific power theory. In addition, the use of a TI in these devices is only one example of its possible implementations in the field of electric power systems.
The remainder of the paper consists of five sections, which cover the following issues: the topology of the adaptive passive compensator, the basics of operation of a TI device, a field simulation model of the TI, the results of testing a laboratory prototype of an electrical power system with the inductor, and the conclusions.

2. Adaptive Passive Devices for Improving the Quality of Electricity

A fixed-parameter passive compensator improves the power factor of a supply source when its load also has fixed parameters. When these parameters vary, the effectiveness of operation of this type of compensator is lowered [1,3,13,18], meaning that an adaptive compensator is needed instead. A compensator has adaptive properties if it can be

adjusted to changes in both the load power and the power line. This can be carried out by switches or through the use of reactive elements with controllable parameter values. Adaptive compensators can be built in the form of reactive compensators with semi-controlled devices, such as thyristors, or as switching compensators, commonly known as active power filters (APF), in which different types of fully controlled devices are used in the power stage of the compensator. However, when the load power is very high, as is common for large manufacturing plants, APFs are not usually sufficient. A block diagram of an exemplary electric system with a generalised adaptive passive compensator (APC) [1,3,13] is shown in Figure 1a.

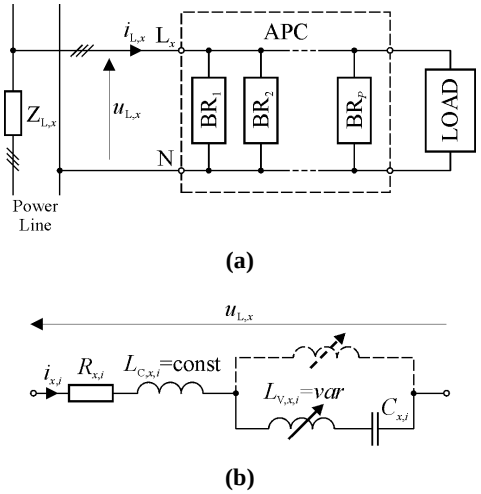

Figure 1. Diagrams of (**a**) an adaptive passive compensator and (**b**) a single branch.

The APC contains P branches ($BR_i : i = 1, 2, \ldots, P$) that can be connected in different ways, typically in parallel, as shown in Figure 1a.
An example of the topology of a single branch using a TI is shown in Figure 1b. As a result of the operation of the tuned inductor, the impedance of this circuit can vary, as follows:

$$\underline{Z_{x,i}} = \frac{U_{\mathrm{L},x}}{\underline{I_{\mathrm{L},x}}} = \mathrm{var} : x = 1, 2, 3, \tag{1}$$

where x is the phase number in the power grid line.
However, it should be clearly stated, that the APC is not, in formal terms, a fully passive system (as follows from its scheme), since a passive compensator can also use different kinds of single power electronics switches or even complete power electronics converters. These devices are necessary to control TIs, and their role in this type of power system is explained, in detail, in the following section.

3. Principle of Operation of a Tuned Inductive Device

Formally, the inductance of the coil is defined by the following formula [19]:

$$L = \frac{\Phi_{\mathrm{M}}}{i}, \tag{2}$$

where: Φ_{M} is the total magnetic flux that is excited in the coil by the current (i), flowing in the coil's winding.
Based on Equation (2), for the implementation of an adjustable magnetic device the circuit with two magnetically coupled coils was used, as shown in Figure 2.

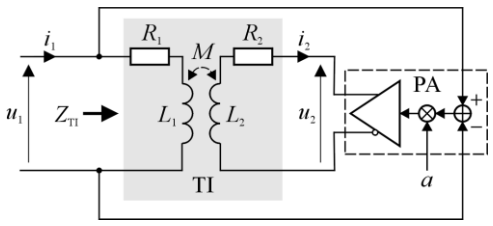

Figure 2. Operation of a circuit with an adjustable magnetic device.

This circuit consists of two main elements; the first of these is the transformer (TI block), which has a working air-gap in the magnetic core. The width of this air-gap influences the value of the magnetic coupling factor (k). The second element

is the power amplifier (PA block) with adjustable gain factor (a), which powers the secondary winding of the transformer. As a result of the operation of the PA block the magnetic flux in the core of the transformer can be amplified or weakened, which causes a change in the equivalent impedance ($\underline{Z_{\mathrm{TI}}} = R_{\mathrm{TI}} + \mathrm{j}X_{\mathrm{TI}}$) of the circuit, when seen from the power source (u_1) side. The value of this impedance depends on the actual values of the parameters of the circuit, and, in particular, the parameter a .

The value of the equivalent impedance of this circuit was calculated based on an analysis of the properties of two magnetically coupled circuits. The initial assumptions made here did not take into account the natural nonlinearity of the ferromagnetic core of the transformer and the voltage excitation (u_1) was assumed to be sinusoidal.

In this case, the pair of equations, describing the voltage and current relations in the circuit, is as follows:

$$\underline{U_1} = R_1\underline{I_1} + \mathrm{j}X_1\underline{I_1} + \mathrm{j}X_{\mathrm{M}}\underline{I_2}\,, \tag{3}$$

$$\underline{U_2} = R_2\underline{I_2} + \mathrm{j}X_2\underline{I_2} + \mathrm{j}X_{\mathrm{M}}\underline{I_1}\,, \tag{4}$$

where: R_1 , R_2 are the resistances of the transformer windings, and X_1 , X_2 , and X_{M} are the self- and mutual reactances of the circuit, respectively.

Setting $\underline{U_2} = a\underline{U_1}$ (where a =const and, theoretically, $-\infty < a < \infty$), the Equations (3) and (4) were transformed to obtain the following formula for the value of $\underline{Z_{\mathrm{TI}}}$:

$$\underline{Z_{\mathrm{TI}}} = \frac{\underline{U_1}}{\underline{I_1}} = \frac{R_1 + \mathrm{j}X_1 + \dfrac{X_{\mathrm{M}}^2}{R_2 + \mathrm{j}X_2}}{1 - a\dfrac{\mathrm{j}X_{\mathrm{M}}}{R_2 + \mathrm{j}X_2}}\,, \tag{5}$$

where:

$$X_{\mathrm{M}} = k\sqrt{X_1 X_2}\ :\ 0 \le k \le 1\,. \tag{6}$$

From Equations (5) and (6), the following expression was obtained, in which the value of the equivalent impedance (Z_{TI}) is dependent on the other parameters of this circuit:

$$\underline{Z_{\mathrm{TI}}} = \frac{R_1 + \mathrm{j}X_1 + k^2\dfrac{X_1 X_2}{R_2 + \mathrm{j}X_2}}{1 - \mathrm{j}ak\dfrac{\sqrt{X_1 X_2}}{R_2 + \mathrm{j}X_2}}\,. \tag{7}$$

To extract the X_{TI} component of the impedance, both resistances were neglected. In this case, Equation (7) has the form:

$$\underline{Z_{\mathrm{TI}}} = \mathrm{j}\frac{1 - k^2}{1 - ak\sqrt{\dfrac{X_1}{X_2}}}X_1\,. \tag{8}$$

Assuming then the equality of both reactances, i.e., $X_1 = X_2 = X$, Equation (8) has the following final form:

$$\underline{Z_{\mathrm{TI}}} = \mathrm{j}\frac{1 - k^2}{1 - ak}X\,. \tag{9}$$

The plots of magnitude (as a value of X_{TI} , related to X) and phase component (φ_{TI}) of Equation (9), vs. a , while k =const, is shown in Figure 3. In order to better visualization the details of the curves, the gain factor (a) variation was limited to the range of $<0, \dfrac{2}{k}>$. Also, values of reactance, for characteristic values of the gain factor, are shown at the magnitude curve, as points. In relation to the right vertical axis of the figure, the abbreviation “el. deg.” denotes the “electrical degree”.

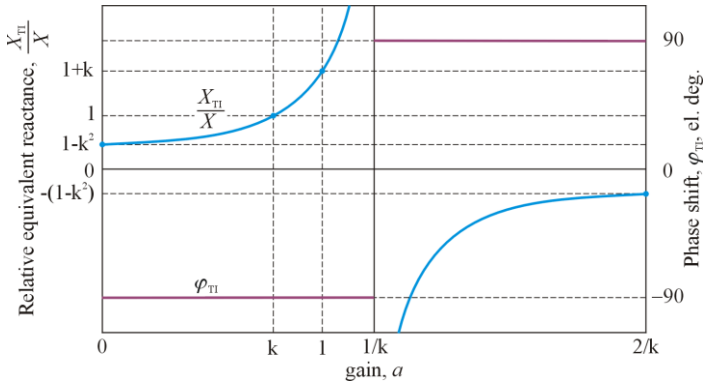

Figure 3. Plots of magnitude (as a value of X_{TI}, related to X) and phase component (φ_{TI}) of Z_{TI}, vs. a, while k =const.

These curves show singular points at $a=\frac{1}{k}$. Thus, the value of X_{TI}, in relation to the gain factor, lies within intervals given by the expressions:

$$X_{TI}\begin{cases} >0 : a<\frac{1}{k} \\ \to \pm\infty : a=\frac{1}{k} \\ <0 : a>\frac{1}{k} \end{cases}. \tag{10}$$

From circuit theory [19], the interpretation of Equations (9) and (10) is that, depending on the value of the gain factor, the adjustable magnetic device is equivalent to a variable inductance coil or a variable capacitance capacitor. However, in the latter case, it is obvious that it cannot form a capacitor as such, due to it does not has the ability to store an electric charge. Nevertheless, in a real circuit, that description is given by Equations (5) and (7), and due to the presence of the resistances, the aforementioned phase shift is different from ±90°. For simplicity, it was again assume the equality of both reactances ($X_1=X_2=X$) and both resistances ($R_1=R_2=R$). In such a case the Equation (7) takes the following form:

$$\underline{Z_{TI}}=R\frac{1+\left(\frac{X}{R}\right)^2\left(k^2-1\right)+\mathrm{j}2\frac{X}{R}}{1+\mathrm{j}(1-ak)\frac{X}{R}}. \tag{11}$$

For easier interpretation of the circuit features, the time constant of the TI block (τ_{TI}) was used in the next expression. In this case, Equation (11) takes the form:

$$\underline{Z_{TI}}=R\frac{1+(\omega\tau_{TI})^2\left(k^2-1\right)+\mathrm{j}2\omega\tau_{TI}}{1+\mathrm{j}(1-ak)\omega\tau_{TI}}:\ \tau_{TI}=\frac{L}{R}. \tag{12}$$

Figure 4 shows the phase shift, based on Equation (12), vs. a, for $\omega\tau_{TI}$ = const. The variation in the gain factor was limited to the range $<0,\frac{2}{k}>$.

From the point of view of the properties of the TI block, its operation can be divided into two types, based on the sign of the phase shift. If this sign is negative, the TI operates in the "tuned inductor mode" (TIM), while in the opposite case it operates in the "tuned capacitor mode" (TCM), as illustrated in Figure 4.

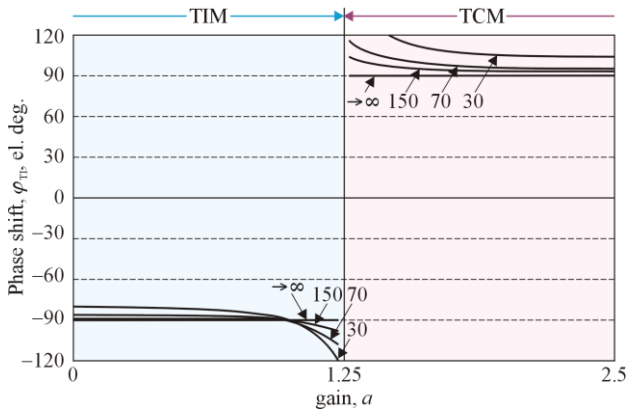

Figure 4. Plots of the phase shift (φ_{TI}) vs. a , for $\omega\tau_{TI}$ = 30, 70, 150, and $\omega\tau_{TI} \to \infty$.

A comparison with Figure 3b clearly shows phase errors, the values of which increase as the resistance increases, which, in turn, results in a decrease in the value of $\omega\tau_{TI}$.

4. Tuned Inductor's Design

The aim of the research was to obtain technical details of the inductor, which are necessary for the design of its a laboratory prototype. At the initial stage simulation studies of the TI field model were conducted, using Maxwell Environment [20] and in-house optimisation software [21]. This study showed that to achieve the assumed value for the inductance of the TI, a sophisticated design of its magnetic circuit was necessary. As a result, a three-column magnetic core was chosen for the model of the transformer. Each of the columns was equipped with a working air-gap with a width equal to g . In the model, ferrite E-shapes (manufactured by MAGNETICS Inc., catalogue number: OT49928EC), made of T-type ferrite material [22], were used. The model of the core was composed of four of these shapes. The primary coil was wound on the central column of the device, while the secondary coil was divided into two equal parts and wound on both external columns. To simplify the modelling procedure it was also assumed that the number of turns were equal for all of the coils, i.e., $z_1 = z_{21} = z_{22}$, as shown in Figure 5.

Taking into account the potential fields of application of the TI, reported in previous works [23,24], values of X = 4.50 mH and k = 0.80 were assumed. These aforementioned works also presented details of the whole inductor's research procedure.

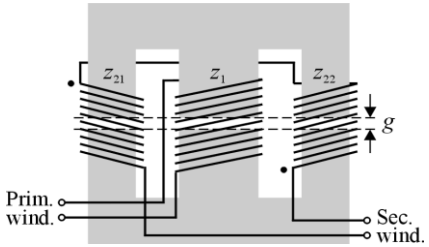

Figure 5. Diagram, showing the design of the tuned inductor.

5. Laboratory Tests and Discussion

5.1. Tests of a Laboratory Prototype of the Adjustable Magnetic Device

In the power stage of the tested circuit a P3-5-550MFE LABINVERTER [25] was implemented. This device was designed for applications in advanced R&D power electronics systems. The control module of the LABINVERTER comprised an ALS-G3-1369 evaluation board [25] with a 32-bit digital signal processor (Analog Devices Inc., ADSP-21369 SHARC®). In turn, this board is dedicated such power electronics applications, which require a CPU with high computation power and a PWM pattern with high resolution, among others.

The aim of the first part of the research was to confirm the parameters for the laboratory prototype of this device, in relation to the field model of the inductor. A photograph of the inductor is shown in Figure 6.

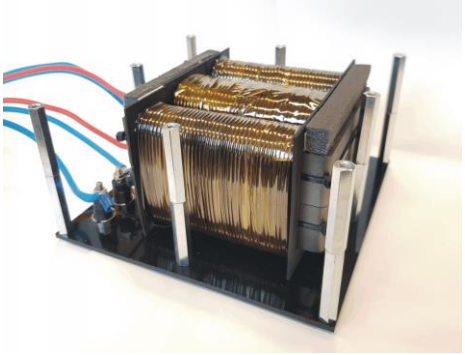

Figure 6. The laboratory prototype of the tuned inductor.

The methodology used to measure the inductance was described in detail in a previous paper [26], and it is discussed this here very briefly, only for the convenience of the reader. This methodology depended on the observation of voltage and current waveforms in the circuit with the TI, as shown in Figure 7. These waveforms were then used as the basis for calculating the inductance of the TI.

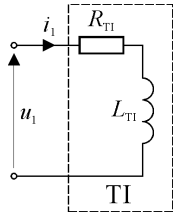

Figure 7. Circuit, used to calculate the equivalent inductance of the TI block.

The general formula, that describes the voltage and current waveforms in this circuit, in the time domain, is as follows:

$$u_1(t) = R_{TI} i_1(t) + L_{TI} \frac{\mathrm{d}i_1(t)}{\mathrm{d}t}. \tag{13}$$

For practical purposes, the resistance of the circuit was ignored and the supply voltage was assumed to be a rectangular function of time, meaning that the current waveform will be a linear function of time, i.e., a first-order polynomial. As a result, the value of the equivalent inductance of the TI can be calculated using the formula:

$$L_{TI} = \frac{\Delta u_1}{\Delta i_1} \Delta t, \tag{14}$$

where Δu_1, Δi_1, and Δt represent the changes in the voltage, current, and time, respectively.

The assumption that neglecting the resistance TI does not result in a significant value of error, when calculating the inductance value, holds true [26] under the condition that the measurement time (Δt) is much shorter than the time-constant of the circuit, i.e.:

$$\Delta t << \frac{L_{TI}}{R_{TI}}. \tag{15}$$

This statement was confirmed experimentally, based on a wide range of tests of numerous types of inductive devices; the examples of such works are [23,24,26].

As a result of laboratory investigations of the TI model, the following values were obtained for the parameters of the device:

- Number of turns: $z_1 = z_{21} = z_{22} = 80$;
- Air gap width: $g = 2.0$ mm;
- Inductance (related to the quasi-linear range of the magnetic core operation) of the secondary winding (open): $L_{TI,0} = 4.55$ mH;
- Inductance of the secondary winding (short-circuited): $L_{TI,1} = 1.64$ mH;
- Winding resistance: $R_1 = 110$ mΩ, $R_2 = 220$ mΩ.

Based on these assumptions for the TI model, and from the results of laboratory investigations, the value of the coupling factor was calculated as $k = 0.80$. The relationship between $L_{TI,0}$ and $L_{TI,1}$ is then equal to 2.77.

5.2. Tests of the Electric System with a Tuned Inductor: Basic Configuration

Figure 8 shows a block diagram of the laboratory circuit used to test the operation of the tuned magnetic device (TI) in the basic configuration. The aim of these tests was to confirm the assumed features of the TI as an adjustable magnetic device, i.e., its ability to change the equivalent inductance and more.
The measurement circuit consisted of the following main blocks and components:

- Power line;
- EMI filter (EMIF);
- Auto-transformer (ATR);
- Transformer (TR);
- Tested magnetic device (TI);
- H-bridge, voltage source inverter (VSI);
- LCL type filter (FLT), included at the output of the inverter;
- Inverter control module (CM);
- Isolated current and voltage transducers (CT and VT, respectively);
- Regulated DC laboratory power supply (PSP).

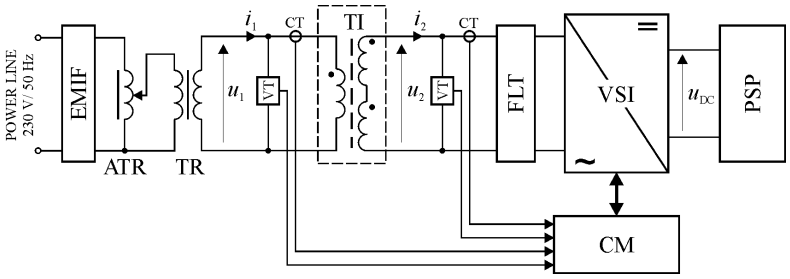

Figure 8. Block diagram of the measurement circuit, used for testing the tuned inductor – basic configuration.

The VSI and FLT blocks made up the precision power electronics voltage controlled voltage source (VCVS), which powered the secondary winding of the transformer (the TI block).
A wide range of tests were carried out on the system with the inductive device, using 'hardware-in-the-loop' modelling. Most of the waveforms were recorded using the PLOT function of DSP Emulator software, which is included in the VisualDSP++® environment [27]. The PLOT function allows for graphic visualisation of data, stored as objects in the C/C++ language, such as numerical arrays. A C/C++ compiler is one of the main components of VisualDSP++®.
The gain coefficient of the PA was varied within the interval <0, 2.5>. During tests, the RMS value of the supply voltage (u_1) was set to 7 V. Figure 9 shows the most characteristic waveforms for the tested circuit, i.e., u_1 and i_1, as function of a, over time. The lower part of this figure shows details of the voltage and current waveforms, including the phase relationship between these two quantities. It can be seen clearly that, after a exceeds the value of $1.0/k$, the circuit changes its character from an inductive to a capacitive.

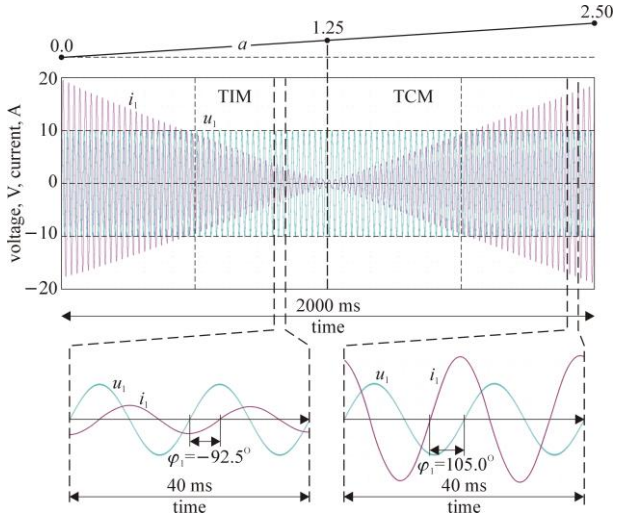

Figure 9. Waveforms for the supply voltage and current in the primary winding of the tuned inductor, relative to the gain coefficient, as a function of time.

5.3. Tests of the Electrical System with a Tuned Inductor: Extended Configuration

A block diagram of the laboratory circuit used to test the operation of the TI in the extended configuration is shown in Figure 10. The aim of these tests was to confirm the features of the TI as a component of a tunable parallel resonant circuit.

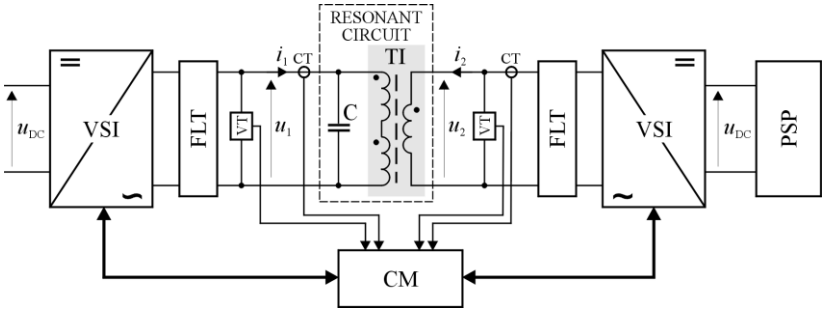

Figure 10. Block diagram of the measurement circuit, used to test the tuned inductor in extended tests, with a parallel resonant section.

The resonant circuit was composed of TI and capacitance elements (shown in the figure by the dashed line), where the capacitance consisted of a set of high-quality polypropylene-film capacitors with C = 300 μF ±1 %. The gain coefficient of the PA was varied in the interval <0, 1.25>. During these tests, the RMS value of the supply voltage (u_1) was set to 10 V, and its basic frequency was equal to 150 Hz (i.e., the third harmonics of the power line voltage). Thus, this circuit was demanded implementation of the second VCVS block.

Figure 11 shows the characteristic waveform for the circuit (i_1) and a plot of a vs. time. A curve of the equivalent inductance vs. a is also shown. From the figure, the moment at which parallel resonance occurs is clearly visible. This results from the given value of the equivalent inductance (reactance) of the TI, which is a function of the gain factor.

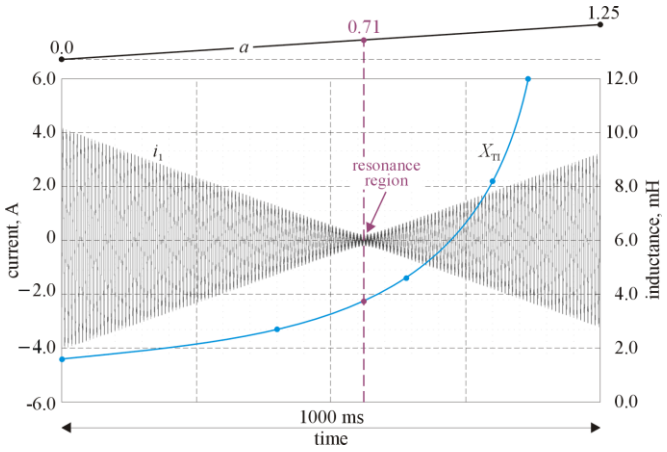

Figure 11. Waveform of the current in the primary winding of the tuned inductor, relative to the gain coefficient, as a function of time.

5.4. Discussion

The test results show that from the point of view of the relationship between the voltage and current, the inductive device presented here is able to operate in two modes, as either a tuned inductor or a tuned capacitor. However, the actual values of the equivalent inductance ('capacitance') of TI were affected by an error of up to 15.0%. The size of this error depends on the gain coefficient, which may result in a decrease in the equivalent reactance of the device. The error arises from factors such as the presence of resistance in the real circuit, the difference between the theoretical and actual voltage values in the secondary circuit of the transformer (caused by the gain error of the power amplifier), and the presence of a ripple component in this voltage, which is caused by the pulse-width modulation (PWM), used to control the power electronics inverters. The phase shift of the primary current from the supply voltage is different from the desired value (i.e., −90° or +90°) depending on the mode of operation of the device, since the circuit contains the aforementioned TI winding resistances. The value of the phase error was in the range 2.7–16.7%, depending on the actual value of the gain coefficient. Nevertheless, these tests proved that the proposed device can be an effective element of a tunable resonant circuit, by determining its main property in the form of the value of the self-resonance frequency. In this case, the error in the value of the resonance frequency as a function of the gain factor was no greater than 1% of the expected (i.e., theoretical) value. This is within the range of error of the measuring instruments used. It should be noted that, in the simplified version, the tunable inductive device was tested in a real electric system, including the DC power supply, equipped with the function of active compensation of reactive and distortion power [24].

Taking into account tests results (especially, included in the Section 5.2) it can be concluded that the operation of the magnetic element presented in this work is similar to that of a gyrator [28], as an inverter of impedance.

6. Conclusions

This work has presented the principles of operation and test results for models of electrical systems including a variable inductance device. The operation of the device was based on the interaction between a pair of coupled fluxes, but without relying on the natural nonlinearity of the ferromagnetic circuit, as in most previous studies (e.g., [30]). Instead, the interaction between two magnetic fluxes in the quasi-linear range of operation of the ferromagnetic core was exploited. Experimental results confirmed the possibility of obtaining the desired reactance value in a smooth manner, as a result of controlling the flux in the inductor, with relative error of no more than 15%. In the author's opinion, this value can be considered satisfactory in view of the complexity of both the magnetic circuit of the device and the entire system with this device. In addition, tests of a tunable resonant circuit confirmed the utility of this device in a power electrical system. Nevertheless, further tests of the inductor are necessary, to assess the impact of non-linearity of the real magnetic core and power losses on its operation.

It seems that the proposed device offers an attractive solution, particularly for electrical power systems with adaptive features, such as those used to improve the quality of electricity and for energy transmission via power lines. However, these applications for the inductor also need further research, using simulation and laboratory models.

References

1. Rashid, M.H. *Power Electronics Handbook*; Elsevier Ltd.: Oxford, UK, 2018.
2. Akagi, H.; Watanabe, E.H.; Aredes, M. *Instantaneous Power Theory and Applications to Power Conditioning*; John Wiley & Sons: Hoboken, NJ, USA, 2017; ISBN: 9781118362105.
3. Pasko, M.; Buła, D.; Dębowski, K.; Grabowski, D.; Maciążek, M. Selected methods for improving operating conditions of three-phase systems working in the presence of current and voltage deformation—Part I. *Arch. Electr. Eng.* **2018**, *67*, 591–602. https://doi.org/10.24425/123665.
4. Trinh, Q.; Lee, H. An enhanced grid current compensator for grid-connected distributed generation under nonlinear loads and grid voltage distortions. *IEEE Trans. Ind. Electron.* **2014**, *61*, 6528–6537. https://doi.org/10.1109/TIE.2014.2320218.
5. Hamdy, M.; Abdelaziz, A.Y.; Ray, P.; Attia, M.A. Comparison between flexible AC transmission systems (FACTs) and filters regarding renewable energy systems harmonics mitigation. *Int. J. Emerg. Electr. Power Syst.* **2021**, *23*, 211–220. doi.org/10.1515/ijeeps-2020-0274.
6. Benchabira, A.; Khiat, M. A hybrid method for the optimal reactive power dispatch and the control of voltages in an electrical energy network. *Arch. Electr. Eng.* **2019**, *68*, 535–551.
7. Yang, Y.; Ma, J.; Ho, C.; Zou, Y. A new coupled-inductor structure for interleaving bidirectional DC-DC converters. *IEEE J. Emerg. Sel. Top. Power Electron.* **2015**, *3*, 841–849. https://doi.org/10.1109/JESTPE.2015.2443178.
8. Yang, C.; Liu, Y.; Tseng, P.; Pan, T.; Chiu, H.; Lo, Y. DSP-based interleaved buck power factor corrector with adaptive slope compensation. *IEEE Trans. Ind. Electron.* **2015**, *62*, 4665–4677. https://doi.org/10.1109/TIE.2015.2400421.
9. Onal, Y.; Sozer, Y. Bridgeless SEPIC PFC converter for low total harmonic distortion and high power factor. In Proceedings of the Applied Power Electronics Conference and Exposition (APEC), Long Beach, CA, USA, 20–24 March 2016; pp. 2693–2699.
10. Liu, J.; Xu, W.; Chan, K. W.; Liu, M.; Zhang, X.; Chan, N. H. L. A Three-phase single-stage AC–DC wireless-power-transfer converter with power factor correction and bus voltage control. *IEEE J. Emerg. Sel. Top. Power Electron.* **2020**, *8*, 1782–1800. https://doi.org/10.1109/JESTPE.2019.2916258.
11. Masetti, C. Revision of European Standard EN 50160 on power quality: Reasons and solutions. In Proceedings of the 14th International Conference on Harmonics and Quality of Power-ICHQP, Bergamo, Italy, 26–29 September 2010.
12. Popescu, M.; Bitoleanu, A.; Linca, M.; Suru, C.V. Improving power quality by a four-wire shunt active power filter: A case study. *Energies* **2021**, *14*, 1951. https://doi.org/10.3390/en14071951.
13. Czarnecki, L.; Almousa, M. Adaptive balancing by reactive compensators of three-phase linear loads supplied by nonsinusoidal voltage from four-wire lines. *Am. J. Electr. Power Energy Syst.* **2021**, *10*, 32–42. https://doi.org/10.11648/j.epes.20211003.11.
14. Ye, T.; Dai, N.; Zhu, M. Optimise the series LC design of a quasi-proportional-resonant controlled hybrid active power filter for harmonic compensation. In Proceedings of the 11th Conference on Industrial Electronics and Applications (IEEE ICIEA), Hefei, China, 5–7 June 2016; pp. 624–629. https://doi.org/10.1109/ICIEA.2016. 7603659.
15. Depenbrock, M.; Marshal, D.A.; Wyk, J.D. Formulating requirements for universally applicable power theory as control algorithm in power compensators. *Eur. Trans. Elect. Power ETEP* **1994**, *4*, 445–456.
16. Qiao, X.; Bian, J.; Chen, C.; Li, H. Comparison and analysis of reactive power compensation strategy in power system. In Proceedings of the IEEE Sustainable Power and Energy Conference (IEEE iSPEC), Beijing, China, 21–23 November 2019, pp. 689–692. https://doi.org/10.1109/iSPEC48194.2019.8975301.
17. Benysek, G.; Pasko, M., Eds. *Power Theories for Improved Power Quality*; Springer-Verlag: London, UK, 2012.
18. Lee, Y.; Song, H. A reactive power compensation strategy for voltage stability challenges in the Korean power system with dynamic loads. *Sustainability* **2019**, *11*, 326. https://doi.org/10.3390/su11020326.
19. *Magnetic Circuits and Transformers: A First Course for Power and Communication Engineers.* MIT Department of Electrical Engineering, One Broadway 12th Floor Cambridge, MA 02142, USA, November 15, 1977, ISBN: 9780262630634.
20. ANSYS Software. Available online: https://www.ansys.com/products/electronics/ansys-maxwell (accessed on 30 December 2022).
21. Knypiński, Ł.; Nowak, L.; Demenko, A. Optimisation of the synchronous motor with hybrid permanent magnet excitation system. *COMPEL* **2015**, *34*, 448–4552. https://doi.org/10.1108/COMPEL-08-2014-0216.
22. MAGNETICS Inc. Available online: https://www.mag-inc.com/home (accessed on 30 December 2022).
23. Gwóźdź, M.; Wojciechowski, R.M. Use of the tuned multi-legs inductor in the device for improving a quality of electric energy. In Proceedings of LV Symposium on Electrical Machines (SME), Poznań, Poland, 27–28 April 2022; pp. 1–2.
24. Ciepliński, Ł.; Gwóźdź, M.; Wojciechowski, R.M. Application of a tuned inductor in a DC power supply with an active compensation function. *Energies* **2022**, *15*, 6108. https://doi.org/10.3390/en15176108.

25. ALFINE-TIM. Available online: http://analog.alfine.pl/oferta/produkty-alfine/systemy-uruchomieniowe (accessed on 30 December 2022).
26. Gwóźdź, M. The application of tuned inductors in electric power systems. *Energies* **2022**, *15*(22), 8481. https://doi.org/10.3390/en15228481.
27. VDSP++ 5.0, Run-Time Library Manual for SHARC® Processors, Revision 1.5; January 2011, Part Number 82-000420-09, Analog Devices, Inc.: Norwood, MA, USA, One Technology Way. Available online: https://www.analog.com/media/en/dsp-documentation/software-manuals/50_21k_rtl_mn_rev_1.5.pdf (accessed on 30 December 2022).
28. Deliyannis, T.; Sun, Y.; Kel Fidler, J. *Continuous-Time Active Filter Design*; CRC Press, 1999; pp. 81-82. ISBN 0-8493-2573-0.